Letters in Applied NanoBioScience
Open-Access Journal (ISSN: 2284-6808)

Article
Volume 13, Issue 1, 2024, 48
https://doi.org/10.33263/LIANBS131.048

Use of 1,2,3-triazole Derivatives as Potential Inhibitors Blood Cancer, 3D-QSAR, Molecular Docking, and *In-silico* Pharmacokinetic and Toxicological Studies

Yassine Koubi [1], Youness Moukhliss [1], Halima Hajji [1], Aziz Mohammed Ajana [1], Hamid Maghat [1], Mohammed Bouachrine [1,2], Tahar Lakhlifi [1,*]

[1] Molecular chemistry and Natural Substances Laboratory, Faculty of Science, University Moulay Ismail, Meknes, Morocco; yassine.koubi@edu.umi.ac.ma (Y.K.); y.moukhliss@edu.umi.ac.ma (Y.M.); hajjilima@gmail.com (H.H.); a.ajanamohammed@fs.umi.ac.ma (M.A.A.); h.maghat@umi.ac.ma (H.M.); tahar.lakhlifi@yahoo.fr (T.L.); bouachrine@gmail.com (M.B.)
[2] Higher School of Technology (HST), Sultan Moulay Sliman University, BP 23000 Beni-Mellal, Morocco; bouachrine@gmail.com (M.B.)
* Correspondence: tahar.lakhlifi@yahoo.fr (T.L.);

Scopus Author ID 6507937108
Received: 8.07.2022; Accepted: 15.08.2022; Published: 25.03.2024

Abstract: Recently, several types of cancer have been rising, and among these types of cancer, blood cancer has become a global problem, hence the discovery of new anticancer agents by computational chemistry. To improve and propose new compounds with anticancer activity, a quantitative three-dimensional structure-activity study (3D-QSAR) on anticancer analogs A 3D QSAR model based on Comparative Molecular Field Analysis (CoMFA) and Comparative Molecular Similarity Index Analysis (CoMSIA) was created. Analysis (CoMFA) and Comparative Molecular Similarity Index Analysis (CoMSIA) were established. Good stability of the model was obtained using the CoMFA model (Q^2= 0.60; R^2=0.97; R=0.75) and the best model CoMSIA (Q^2=0.61; R^2=0.92; R=0.86). The predictive capacity of the developed model was evaluated by external validation using the statistical indices of A. Tropshak. Roy, A. Golbraikh, and an internal validation by the Y-randomization test. The Docking results showing the interest of amino acids Gly31; Cys41 for anticancer activity and the steric and electrostatic field contours of CoMFA model were monitored. Based on this result, 24 molecules with anticancer activity were proposed. Moreover, ADMET outcomes show that this could help develop new cancer drugs.

Keywords: 3D-QSAR; anticancer activity; ADMET study; cancer drug.

© 2024 by the authors. This article is an open-access article distributed under the terms and conditions of the Creative Commons Attribution (CC BY) license (https://creativecommons.org/licenses/by/4.0/).

1. Introduction

Cancer has remained one of the most common causes of death worldwide [1]. According to WHO in 2018, this proliferative potential can cause a genetic predisposition or exposure to an oxygen factor [2]. The development of a tumor involves many stages over time, such as initiation, proliferation, angiogenesis, and metastasis [3]. There are five major families of anticancer drugs to treat cancer diseases, including antimetabolites, natural products, hormones, and antagonists [4]. The subject of anticancer drug development has become an important focus of scientific research [5]. Numerous studies have been carried out by computational chemistry to intervene in the search for new anticancer drugs, and the optimization of the research leads to this type of drug [6]. Moreover, several studies have

explored triazole molecules that have great biological activity against cancer and other diseases, such as antimicrobial [7], Antiparasitic [8], antibacterial [9], Antioxidant [10], and antitubercular [11].

The present study aims to explore the quantitative three-dimensional structure-activity relationship of 21 triazole derivatives. 3D QSAR models were generated by Comparative Molecular Similarity Index Analysis (CoMSIA). [12,13] and the Comparative Molecular Field Analysis (CoMFA) [14]. After a series of statistical validation tests for the CoMFA model, a total of 24 new compounds with a very high activity compared to the literature molecules were proposed [12]. The tested molecules were evaluated using the Docking method [15] and the calculation of ADMET properties and drug-likeness [16].

2. Materials and Methods

In the present investigation, 24 triazole compounds with biological activity against human cancer cell line HTP-1 [12] in pIC_{50} (-Log (IC_{50})) values. The database is divided into two sets; one contains 19 compounds present in the training set, and the other is known as the test set, composed of 5 compounds Table 1.

Table 1. Triazole compounds studied and their observed and predicted anticancer activities.

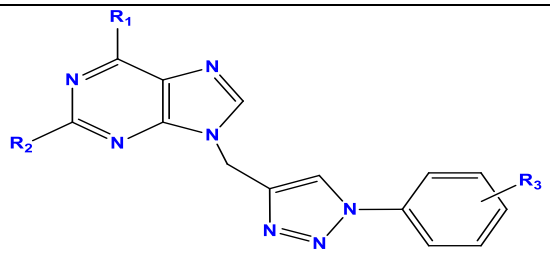

Compound	R_1	R_2	R_3	pIC_{50}
9a	$C_6H_5CH_2NH$-	Pyrolidine	H	7.097
9b	$C_6H_5CH_2NH$-	Piperidine	H	6.097
9c[1]	$C_6H_5CH_2NH$-	Pyrolidine	2-Cl	5.347
9d[1]	$C_6H_5CH_2NH$-	Piperidine	2-Cl	4.469
9e	$C_6H_5CH_2NH$-	Pyrolidine	4-Cl	6.155
9f	$C_6H_5CH_2NH$-	Piperidine	4-Cl	4.728
9g[1]	$C_6H_5CH_2NH$-	Pyrolidine	4-Br	4.548
9h	$C_6H_5CH_2NH$-	Piperidine	4-Br	4.9
9i[1]	$C_6H_5CH_2NH$-	Pyrolidine	2-Br	5.086
9j	$C_6H_5CH_2NH$-	Piperidine	2-Br	5.585
9k	$C_6H_5CH_2NH$-	Pyrolidine	4-F	6.276
9l	$C_6H_5CH_2NH$-	Piperidine	4-F	5.824
9m	$C_6H_5CH_2NH$-	Pyrolidine	2-F	5.602
9n	$C_6H_5CH_2NH$-	Piperidine	2-F	5.495
9o	$C_6H_5CH_2NH$-	Pyrolidine	4-Br, 2-Me	5.244
9p	$C_6H_5CH_2NH$-	Piperidine	4-Br, 2-Me	5.301
9q	$C_6H_5CH_2NH$-	Pyrolidine	3-Br, 2-Me	4.411
9r	$C_6H_5CH_2NH$-	Piperidine	3-Br, 2-Me	4.393
9s	$C_6H_5CH_2NH$-	Pyrolidine	4-OCH_3	4.662
9t	$C_6H_5CH_2NH$-	Piperidine	4-OCH_3	4.585
9u	OH-CH_2-CH_2-NH_2	Pyrolidine	4-F	4.493
9v	OH-CH_2-CH_2-NH_2	Piperidine	4-F	4.542
9w	OH-CH_2-CH_2-NH_2	Pyrolidine	2-Br	4.879
9x[1]	OH-CH_2-CH_2-NH_2	Piperidine	4-Br, 2-Me	4.907

[1] test molecule

2.1. General 3D-QSAR models.

A 3D-QSAR study on a series of 24 methods, this study is based on the analysis of CoMFA and CoMSIA. The CoMFA used in the 3D-QSAR study is the method used for many

years; it is based on the analysis of two descriptors: one is the steric potential calculated by the Lennard-Jones function [26-28], and the other is the electrostatic potential descriptor calculated by the Coulombe function in a three-dimensional structure [29]. The descriptors calculated by the CoMFA method are used to predict the biological activity of compounds and to understand the relationship between the 3D structure and the activity of molecules [26]. Kleber et al. developed a three-dimensional QSAR method called CoMSIA; the latter is based on similarity index analysis instead of grid-based fields, and a SEAL algorithm is adopted for this study [30-32].

In the present work, the 24 compounds were placed in a $2A^0$ resolution cubic grid of the dimension of all compounds with a sp3 hybrid carbon with +1 as a charged probe. The analysis is done in the Sybyl-X 2.00 software.

2.2. Partial Least Squares (PLS) analysis.

The partial least squares method is frequently used for building predictive models when several variables are involved [33,34]. This statistical prediction technique is used to study the predictivity of the models instead of the relationship between the variables [35]. It was developed by Herman Wold as an econometric technique [36].

2.3. Internal validation.

The internal validation of a QSAR model was performed using the correlation coefficient R and the coefficient of determination R^2, the LOO (Leave-One-Out) cross-validation, which is quantified by the coefficient Q^2 [37,38]. However, to provide more reliability to this model, the y-randomization test was used [39]. y-randomization consists of randomizing the biological activities with the descriptors.

2.4. External validation.

The external validation consists of predicting the biological activity of a series of molecules, generally called test series, which are not part of the development series of the model. This validation is characterized by the parameter R^2_{test}. Rtest. [40]. Then, the criteria of A. Golbraikh, A.Tropsha were computed according to the following relationships:

$$r_m{}^2 = r^2\left(1 - \sqrt{r^2 - r_0{}^2}\right) (1)$$

$$r_m{}'^2 = r^2\left(1 - \sqrt{r^2 - r_0{}'^2}\right) (2)$$

r^2_m and r'^2_m represent the validation metrics calculated according to the above equations using observed predicted values and cross-validation without exclusion [41,42].

With r^2 being the squared correlation coefficient between the predicted and the experimental values of the activity, r^2_0 represents the squared correlation coefficient between the predicted value and the zero intercept, and r'^2_0 is the squared correlation coefficient between the experimental intercept and zero. r^2_0 and r'^2_0 can be calculated using the following relationships:

$$r_0{}'^2 = 1 - \frac{\sum(y_i - \hat{y}_i{}^{r_0})^2}{\sum(y_i - \bar{y})^2} (3)$$

A true QSAR model can have a high predictive ability since the regression of ỹ against y is equal to 1. If it is close to ideal, the correlation coefficient R between the actual activities y and the planned activities must be close to 1, and the regressions of y against ỹ or ỹ against

y via the origin, i.e., respectively, must be characterized by at least k or k'close to 1. The slopes k and k' are calculated as follows [43,44]:

$$k = \frac{\sum y_i \tilde{y}_i}{\sum \tilde{y_i}^2} (4)$$

$$k' = \frac{\sum y_i \tilde{y}_i}{\sum y_i{}^2} (5)$$

In the external validation, the coefficient of determination R was calculated, and the criteria A. Golbraikh, A. Tropsha were applied to all the tests to ensure the rigidity and reliability of the studied model.

2.5. Docking method validation protocol.

In this work, the Autodok 1.5.4 software and Autodok Vina [45] were used to validate the CoMFA and CoMSIA contour results by the molecular docking method [46]. The docking first requires the preparation of ligands and proteins. Thus, the ligand and the protein (PDB: 3U8D) in a grid of dimension (x = 45, y = 45, z = 45 has a space of 1A) was placed and defined to replace the folic acid binding site in 1dls; bioactive conformations were simulated using Autodock vina. The results were analyzed using Discovery studio 2016 [47] and PyMol [48] software.

2.6. Pharmacokinetics in silico ADMET and prediction of drug-likeness.

Recently, the discovery of new drugs using computational chemistry should be very useful to evaluate new drugs; it is necessary to use computational techniques such as ADMET and Drug-likeness [49,50]. They are developed to estimate physicochemical and pharmaceutical parameters and toxicity of drugs. This study allowed us to see the percentages of adsorption and distribution as well as parameters related to human metabolism and, excretion and toxicity [51-53]. It is absorbed in the human intestine and passes through the blood-brain barrier and the central nervous system. Metabolism refers to the chemical and biotransformation of drugs in living organisms. The total clearance of drugs and the level of toxicity of molecules [54-56]. The prediction of similarity to designed drugs was evaluated by rules based on Lipinski, Muegge, Veber, and Egan [51].

3. Results and Discussion

3.1. Molecular alignment.

Alignment has become a primordial and obligatory step. Therefore, in the 3D-QSAR study, we chose the 9a molecule as a common structure for alignment and visualization of CoMFA and CoMSIA profiles, representing the smallest IC50 activity value for the experimental series. Alignment and visualization were processed by Sybel-X.2.00 software; the alignment results are shown in Figure 1.

Figure 1. Superposition and alignment of the 24 studied compounds using molecule 9a as a model.

3.2. CoMFA and CoMSIA studies.

3.2.1. CoMFA results.

To investigate the quantitative predictivity and explain the relationship between steric and electrostatic fields with the anticancer biological activity of 24 compounds derived from 1,2,3-triazole. Many statistical validation parameters were calculated from the results provided by the Sybyl-X software. These parameters are R^2, R, Q^2, tF, SEE for the training set and Rtest, R^2_{test}, $\overline{r_m}$ test, Δr^2_{test}, $\Delta r^2_{0\ test}$, $(r^2- r^2_0)/ r^2$, $(r^2- r'^2_0)/ r^2$, K, K' for the test set Table 4 and 5 [54,55].

The value of the coefficient of determination is 0.951. This value is significant for a statistical model, in particular, the coefficient of cross-validation 0.60 with an optimal number of components, which is 4 to generate a CoMFA model. Finally, the value of the standard error state is equal to 0.144 Table 2. The capacity of this model is also confirmed by R_{test}, R^2_{test}, which have 0.957 and 0.978, respectively. The threshold of the parameters of K. Roy, A. Golbraikh, A. Tropsha was respected in Table 3. Thus, the studied model presents good predictive stability of the CoMFA model.

Table 2. PLS statistical results of CoMFA and CoMSIA models in different combinations of molecular fields.

CoMFA		**CoMSIA E/S**	
R	0.951	R	0.860
R^2	0.974	R^2	0.927
Q	0.600	Q	0.610
R^2_{TEST}	0.957	R^2_{TEST}	0.816
R TEST	0.978	R TEST	0.903
SEE	0.144	SEE	0.331
t-F	97.983	t-F	16.526
Stérique	0.748	Stérique	0.464
Électrostatique	0.252	Électrostatique	0.536

Table 3. The parameters of K. Roy, A. Golbraikh, A. Tropsha.

Paramètre	**Équation**	**CoMFA**	**Seuil**
R^2_{test}	$1-\frac{\sum(Y_{obs(test)}-Y_{(test)})^2}{\sum(Y_{obs(test)}-\overline{Y_{obs(test)}})^2}$	0.822	>0.50
$\overline{r_m}$ test	$\frac{\lvert r_m{}^2 - r_m{}'^2\rvert}{2}$	0.771	>0.50
Δr^2_{test}	$\lvert r_m{}^2 - r_m{}'^2\rvert$	-0.007	<0.20
$\Delta r^2_{0\ test}$	$\lvert r_0{}^2 - r_0{}'^2\rvert$	0.097	<0.30
$(r^2- r^2_0)/ r^2$	$\frac{\lvert r^2 - r_0{}^2\rvert}{r^2}$	0.074	<0.10
$(r^2- r'^2_0)/ r^2$	$\frac{\lvert r^2 - r_0{}'^2\rvert}{r^2}$	0.04	<0.10
K	$\frac{\sum Y_{obs}Y_{calc}}{\sum Y_{calc}{}^2}$	0.957	O.85≤K≤1.15
K'	$\frac{\sum Y_{obs}Y_{calc}}{\sum Y_{obs}{}^2}$	1.044	O.85≤ K'≤1.15

3.2.2. CoMSIA results.

For the quantitative predictivity of the CoMSIA model, the same steps were applied to the analysis of the CoMFA model. Therefore, the coefficients of determination and correlation coefficient were first determined and are equal to 0.860 and 0.927, respectively. Then the coefficient of cross-validation was determined to be 0.620. These values are sufficient to build a statistically predictive model. Finally, the values of Fisher and EES tests were determined and equal to 16.526 and 0.333, respectively Table 2, and for the test set, the R^2 test was

calculated equal to 0.903 and R_{test} was 8.166. To give more reliability to the proposed model, the statistical indices of A.Tropshak. Roy, A. Golbraikh were calculated in Table 3. This result is a strong correlation between the steric and electrostatic fields of CoMSIA descriptors and the anticancer activity of 24 compounds derived from 1,2,3-triazoles.

3.3. y-randomisation test.

To give more reliability to the tested model, the y-randomization test was used. This consists of mixing the descriptors and activities between the compounds randomly and re-calculating the statistical parameters. If these statistical randomization parameters match or exceed those of the chosen model, the model is not acceptable. This technique was applied 10 times on the chosen model in Tables 4 and 5. Thus, no test exceeds the statistical parameter table, and the selected model is a significant model and not randomly chosen.

Table 4. Results of the y-randomization test of the CoMFA model.

Model	R	R^2	Q^2
Original	0.951	0.974	0.600
Random 1	0.334	0.111	-0.052
Random 2	0.204	0.041	-0,133
Random 3	0.242	0.058	-0.142
Random 4	0.265	0.070	-0.087
Random 5	0.243	0.059	-0.131
Random 6	0.245	0.060	-0.114
Random 7	0.356	0.127	-0.033
Random 8	0.264	0.069	-0.084
Random 9	0.246	0.060	-0.128
Random 10	0.186	0.034	-0.145

Table 5. Random Models Parameters of the CoMFA model.

Average r	0.259
Average r^2	0.069
Average Q^2	-0.105
cRp^2	0.519

3.4. Graphical interpretation of the CoMFA model.

The contour maps of the CoMFA model for the most active compound 9a are visualized to perform the electrostatic bonding and steric field analysis. These maps are shown in Figure 2. The contour analysis of the CoMFA model reveals that the increase in the biological activity of the selected compounds requires substituting the voluminous groups in the region marked by the green contours (80% contribution). The substitution by voluminous groups is located in the yellow contour regions (20% contribution). Similarly, the contour analysis of the CoMFA steric field displays a large yellow contour in the proximity of R_3 of the triazole compounds, reflecting the presence of the voluminous groups. This proves that compound 9a has smaller H groups in R_3 positions and is more active than compounds 9b, 9e, 9g, 9i, 9k, 9m, 9o, 9q, 9s with the same structure and substitution, including R_1, R_2 (Figure 2), except that it is substituted by groups larger than hydrogen group such as Cl, Br, F, Me, OCH_3. Therefore, for this series's high activity, replacing the R3 positions with smaller groups is necessary.

The blue contour refers to the electrostatic field. It is noted that there is a large blue contour on the region of the R_3 position, which shows that the biological activity of the series can increase by substitution with electropositive groups in this position. This result

is very evident in compound 9a, which is replaced by an H group. This compound is more electropositive than the others of the series, such as 9b, 9e, 9g, 9i, 9k, 9m, 9o, 9q, and 9s.

The red color means that the substitution by electropositive groups in the region of R_2, and R_3 decreases the biological activity of the compounds. This is the case for compounds 9b, 9d, 9f, 9h, 9j, 9n, 9p, and 9r, which have the same substitutions in position R_1 as compound 9a, but their activity is less important because they are replaced by more electropositive groups (pypiridine) than compound 8q which a pyrrolidine group substitutes.

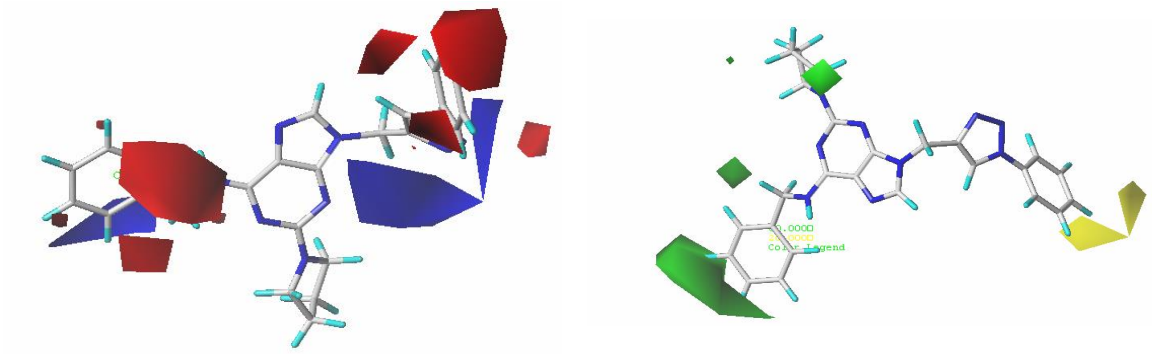

(a) **(b)**

Fig. 2. Electrostatic(a) and steric (b) contour maps of CoMFA analysis of compound 9a.

3.5. Molecular docking.

Molecular docking analysis was used to analyze the interactions between the active site (PDB: 3U8D) of HTP-1 agent proteins and the inhibitor ligan. The active site is constructed by the following amino acids; (Leu2, Phe5, Ile9, Ala17, Ala18, Tyr21, Cys28, Cys44, Phe98, His47, and Asp48;) [57], (Figure 3) (a) shows the interactions between the active site and the most active compound, while (Figure 3) (b) shows the interactions between the least active compound and the active site of the proteins.

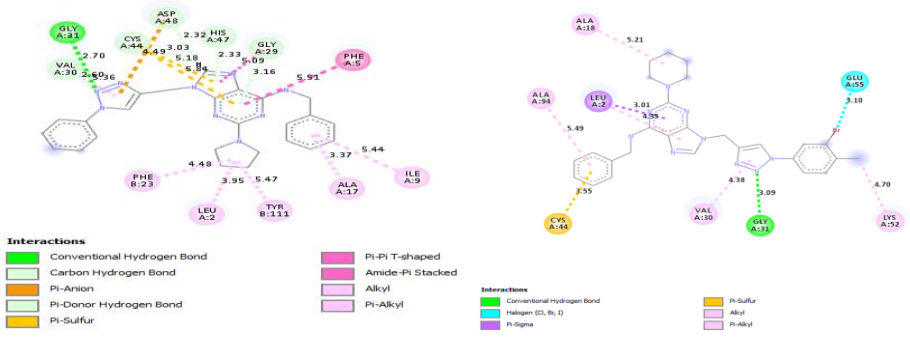

(a) **(b)**

Fig. 3. Types of interactions between the HTP-1 receptor (PDB: 3U8D) and the most active derivative 9a (b) (pIC_{50}=7.09) and the lower active 9r (a) (pIC_{50}=4.39).

Docking analysis indicated that compound 9a, the most active in the series studied, interacts with the active site. The observed interactions are of hydrogen bonding type of Gly31, with the N hydrogen group of the triazole ring. The manure moiety makes carbon-hydrogen bond-type interactions with Gly29 and Asp48, two Pi-Donor Hydrogen Bond interactions with His47 and Cys44, and two sulfide-type interactions with the amino acid Cys44 of Pi-triazole with the active site. The less active compound (9r) displays an active site hydrogen interaction with triazole and Gly31, a classical halogen bond with Glu55.

The most active compound (9a) shows hydrogen-type interactions with Gly31 amino acids, carbon-hydrogen bond, and Pi-Donor hydrogen bond interactions. On the other hand, the less active compound shows halogen-pi-alkyl-type interactions. It can also be observed that the less active compound does not interact with the active site of the protein except with 3 amino acids. In studies of the stability of ligands within active sites of proteins, hydrogen-type interactions, carbon-hydrogen bonding, and Pi-Donor hydrogen bonding are favorable for ligand stability by contributing to Pi-Alkyl and Pi-Sigma interactions. Therefore, it can be concluded that compound 9a is more active than compound 9r due to the non-hydrogen type interactions that were shown in compound 9a.

3.6. Design of new compounds.

The aim of this investigation was to propose new anticancer agents for HTP-1 cells responsible for blood cancer. For this purpose, based on the 3D-QSAR study and the Docking study of the most active compound 9a, new agents for blood cancer inhibition were proposed. In the present study, 24 compounds of triazole derivatives were proposed as new anticancer agents. These compounds are aligned in Sybyl-X, and we chose compound 9a as the common structure. As a result, the activity of the 24 proposed compounds was predicted using the CoMSIA-ES model Table 6.

Table 6. Predicted pIC_{50} based on the CoMFA model for newly designed compounds.

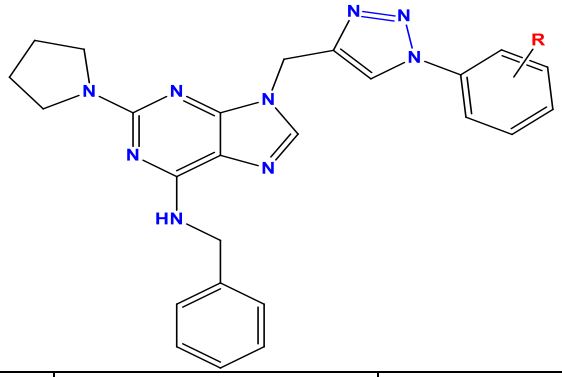

Molecule	pIC_{50}pre	R
X1	9.748	2-C(NH)NH_2
X2	9.05	2,4-C(O)OCH_3
X3	9.049	2,4-C(O)OC_2H_5
X4	8.984	4-NO_2
X5	8.924	4-C(NH)NH_2
X6	8.877	2-C(O)NH_2
X7	8.842	2-CO_2H
X8	8.816	2,4-CO_2H
X9	8.801	4-OH
X10	8.758	2,4-C(NH)NH_2
X11	8.733	2,4-NO_2
X12	8.723	4-C(O)OC_2H_5
X13	8.722	4-C(O)OCH_3
X14	8.711	2-NO_2
X15	8.694	2-CO_2H
X16	8.683	2-C(O)OCH_3
X17	8.608	4-C(O)NH_2
X18	8.602	4-N_2H
X19	8.554	4-COC_2H_5
X20	8.537	2-C(O)OC_2H_5
X21	8.516	2,4-OH
X22	8.418	2,4-N_2H
X23	8.373	2-N_2H
X24	8.237	2,4-COC_2H_5

3.7. ADMET prediction and drug-likeness.

In a series of experiments, 24 proposed compounds showed higher activity than the most active molecule, 9a. The pharmacokinetic parameters ADMET (Absorption, Distribution, Metabolism, Excretion, and Toxicity) and drug binding are calculated to examine the probability of the proposed molecule becoming a drug. The online tool SuissADME [58] was used to predict drug binding properties and the online tool pKCMS [59] was chosen to predict ADMET parameters [60]. If the value of the volume of distribution is greater than 0.45, it is considered high. For the blood-brain barrier (BBB), the LogBB should be between -1 and 0.3; if the LogBB value is less than -1, the compound is poorly distributed, and if the LogBB value is greater than 0.3, the compound is likely to cross the BBB. Targets in the central nervous system (CNS) are characterized by the parameter LogPS. If the value must be between -3 and 2, a LogPS value above 2 is considered a molecule that penetrates the central nervous system (CNS), while a LogPS value below -3 is considered a molecule that penetrates the central nervous system (CNS) poorly.). Internal movement mobile central nervous system [61,62]. According to the analysis of Table 7, all the molecules respect the volume of distribution; the molecule X18 has represented the threshold value of BBB, and the molecules X1, X4, X5, X18, X22, and X23, are present respectable values of the barrier SCN, and the molecules X2, X3, X6, X8. X9, X10, X12, X13, X15, X16, X17, X18, X19, X20, and X24, are molecules capable of moving inside the nervous system according to the results of Table 7, and for AMES, the molecules X2, X3, X6, X7, X8, X10, X12, X13, X15, X16, X17, X18, X19, X20, X21, X22, X23, and X24, are classified as a non-toxic molecule. The conversion of drugs in the human body requires enzymatic metabolism, which can catalyze the chemical biotransformation of drugs. This conversion occurs in several phases in the human body; for this, several metabolites exist [62]. Among these metabolites, cytochrome P450 (CYP450) is very important in drug metabolism as it is the main liver enzyme system involved in phase 1 metabolism (oxidation). 57 CYP genes in 17 families have been identified in humans, but only CYP1, CYP2, CYP3, and CYP4 families are involved in drug metabolism, among which CYPs (1A2, 2C9, 2C19, 2D6, and 3A4) are responsible for more than 90% of the biotransformation of drugs In phase I metabolism [63,64]. Among these families, however, CYP3A4 was the most important inhibitor in this study [65-67]. According to Table 8, the compounds X1, X5, X6, X7, X15, X17, X18, and X21 respected the toxicity parameters of Lipinski, Veber, and Mueggen from two Tables 7,8; most of the new designs were found to be substrates and anticancer drugs.

Table 7. In silico ADMET prediction of newly designed compounds.

Compound	Absorption	Distribution			Metabolism							Excretion	Toxicity
					substrate			Inhibitor					
	Intestinal absorption (human) Numeric (% Absorbed)	VDSS (human) Numeric (Log L/kg)	BBB permeability Numeric (Log BB)	CNS Permeability Numeric (Log PS)	Cyp Categorical (Yes/No)							Total clearance Numeric (Log ml/min/kg)	AMES Toxicity Categorical (Yes/No)
					2D6	3A4	1A2	2C19	2C9	2D6	3A4		
X1	79.63	0.231	-1.401	-2.869	No	Yes	No	Yes	Yes	No	Yes	0.724	Yes
X2	92.53	-0.122	-1.449	-4.304	No	Yes	No	No	Yes	No	Yes	0.821	No
X3	93.95	0.013	-1.448	-3.949	No	Yes	No	No	Yes	No	Yes	0.917	No
X4	91.07	0.137	-1.153	-2.694	No	Yes	No	Yes	Yes	No	Yes	0.579	Yes
X5	79.64	0.226	-1.406	-2.869	No	Yes	No	Yes	Yes	No	Yes	0.813	Yes
X6	86.683	0.071	-1.009	-3.740	No	Yes	No	Yes	Yes	No	Yes	0.792	No
X7	71.861	-0.018	-1.144	-3.723	No	Yes	No	No	Yes	No	No	0.391	No

Compound	Absorption	Distribution			Metabolism							Excretion	Toxicity
					substrate				Inhibitor				
	Intestinal absorption (human) Numeric (% Absorbed)	VDSS (human) Numeric (Log L/kg)	BBB permeability Numeric (Log BB)	CNS Permeability Numeric (Log PS)	Cyp Categorical (Yes/No)							Total clearance Numeric (Log ml/min/kg)	AMES Toxicity Categorical (Yes/No)
					2D6	3A4	1A2	2C19	2C9	2D6	3A4		
X8	47.139	-0.215	-2.038	-4.331	No	No	No	No	No	No	No	0.073	No
X9	87.911	0.213	-0.951X	-3.341	No	Yes	No	Yes	Yes	No	Yes	0.806	Yes
X10	65.437	0.248	-1.691	-3.33	No	Yes	No	No	No	No	Yes	0.627	No
X11	88.289	-0.068	-1.532	-2.874	No	Yes	No	Yes	Yes	No	Yes	0.196	Yes
X12	89.471	-0.007	-1.129	-3.680	No	Yes	No	No	Yes	No	Yes	0.929	No
X13	88.714	-0.029	-1.115	-3.692	No	Yes	No	No	Yes	No	Yes	0.877	No
X14	91.062	0.17	-1.142	-2.694	No	Yes	No	Yes	Yes	No	Yes	0.459	Yes
X15	68.901	0.012	-1.148	-3.653	No	Yes	No	No	Yes	No	No	0.467	No
X16	91.674	-0.037	-1.111	-3.809	No	Yes	No	No	Yes	No	Yes	0.801	No
X17	83.72	0.071	-1.104	-3.669	No	Yes	No	Yes	Yes	No	Yes	0.831	No
X18	91.021	0.237	0.087	-1.049	No	Yes	No	Yes	Yes	No	Yes	0.691	No
X19	89.471	-0.007	-1.129	-3.680	No	Yes	No	No	Yes	No	Yes	0.929	No
X20	92.432	-0.016	-1.124	-3.797	No	Yes	No	Yes	Yes	No	Yes	0.851	No
X21	79.713	0.142	-1.643	-3.789	No	Yes	No	Yes	Yes	No	Yes	0.635	No
X22	88.019	0.304	-1.904	-2.634	No	Yes	No	Yes	Yes	No	Yes	0.382	No
X23	90.98	0.231	-1.052	-2.56	No	Yes	No	Yes	Yes	No	Yes	0.582	No
X24	94.029	-0.073	-1.472	-4.272	No	Yes	No	No	Yes	No	Yes	0.916	No

Table 8. Prediction of drug similarity of the 24 compounds based on Lipinski, Veber, Veber, and Egan, and their synthetic accessibility.

Compound	Lipinski	Veber	Egan	Muegge	Synthetic accessibility
X1	YES	YES	NO	YES	4.05
X2	NO	NO	NO	YES	4.33
X3	NO	NO	NO	YES	4.59
X4	YES	YES	NO	YES	3.58
X5	YES	YES	NO	YES	3.97
X6	YES	YES	YES	YES	3.98
X7	YES	YES	YES	YES	3.92
X8	NO	NO	NO	NO	4.07
X9	YES	YES	YES	YES	3.78
X10	NO	NO	NO	NO	4.28
X11	NO	NO	NO	NO	4.07
X12	NO	YES	YES	YES	4.09
X13	NO	YES	YES	YES	3.96
X14	YES	YES	NO	YES	3.95
X15	YES	YES	YES	YES	3.84
X16	NO	YES	YES	YES	4.05
X17	YES	YES	YES	YES	3.88
X18	YES	YES	YES	YES	3.90
X19	NO	YES	YES	YES	4.09
X20	NO	YES	YES	YES	4.18
X21	YES	YES	YES	YES	3.84
X22	NO	NO	NO	NO	4.09
X23	YES	YES	YES	YES	3.95
X24	NO	NO	NO	NO	4.59

4. Conclusions

In order to develop novel anticancer inhibitors, the relationship between the structure and activity of the reported 1,2,3-triazole inhibitors was investigated statistically using 3D-QSAR technology. Through a battery of tests, we performed 3D QSAR and molecular docking studies as well as ADMET. In this study, we developed two models to predict cancer activity, in which we kept the CoMFA model, selected after multiple types of validation, such as: B. Internal validation (R2, R, Q2, SEE, t-F), external validation (R_{test}, R^2_{test}, A. Golblaikh, A. Tropsha criteria) and test y randomization techniques to ensure the reliability of our model. We

determined molecular docking between the most active molecule (9a) and the least active molecule (9b). Results Figure 3 shows that 1,2,3-triazole derivatives act on the active site of HTP-1. The type of interaction of the ligand with the active site of HTP-1 (van der Waals, conventional hydrogen bonds, carbon-hydrogen bonds), which In good agreement with the chemical properties of 1,2,3-triazole determined by the scan profile

These results also suggest that bond-like interactions play a very important role in validating anticancer drugs. In addition, the molecular docking results were analyzed, and CoMFA profiling allowed us to propose 24 novel inhibitors with very high pIC_{50pred} that could be used as anticancer inhibitors. In addition, each engineered compound was subjected to ADMET standard pharmacokinetic parameter calculations to assess drug-like capability. These new compounds showed high reliability in their anticancer biological activity and also satisfied most ADMET parameters in silico and drug similarity methods. Finally, these new antimicrobials proposed in this study could be good candidates for treating blood cancers.

Funding

This research received no external funding.

Acknowledgments

This research has no acknowledgment.

Conflicts of Interest

The authors declare no conflict of interest.

References

1. Sachs, C.; Tebacher-Alt, M.; Mark, M. Aplasie cutanée congénitale et antithyroïdiens de synthèse au cours de la grossesse, *Ann. Dermatol. Venereol.* **2016**, *143*, 423-435, https://doi.org/10.1016/j.annder.2016.02.018.
2. Nussbaumer, S.; Bonnabry, P.; Veuthey, L.; Fleury, S. Analysis of anticancer drugs: A review *Talanta* **2011,** *85*, 2265–2289, https://doi.org/10.1016/j.talanta.2011.08.034.
3. Saxena, S.; Singh, R.K. Chemokines orchestrate tumor cells and the microenvironment to achieve metastatic heterogeneity. *Cancer and Metastasis Reviews* **2021,** *30*, 447–476, https://doi.org/10.1007/s10555-021-09970-6.
4. Monneret, C. Impact actuel des produits naturels sur la découverte de nouveaux médicaments anticancéreux. *Annales Pharmacetique Francaises* **2010**, *68*, 218-232, https://doi.org/10.1016/j.pharma.2010.04.004.
5. Salehi-Rad, R.; Li, R.; Paul, M. K. The biology of lung cancer: development of more effective methods for prevention, diagnosis, and treatment. *Clinics in Chest Medicine* **2020,** *41*, 25-38, https://doi.org/10.1016/j.ccm.2019.10.003.
6. El Mchichi, L.; El-Aissouq, A.; Kasmi, R.; Belhassan, A.; El-Mernissi, R.; Oussama, A.; Bouachrine, M.; Lakhlifi, T. In silico design of novel Pyrazole derivatives containing thiourea skeleton as anticancer agents using: 3D QSAR, Drug-Likeness studies, ADMET prediction and molecular docking, *Materials Today Proceedings*. **2021,** *45*, 7661–7674, https://doi.org/10.1016/j.matpr.2021.03.152.
7. Akentieva, N.P.; Shushanov, S.S.; Gizatullin, A.R.; Prikhodchenco, T.R.; Shkondina, N.I.; D'Agaro, E. The effect of plant extracts Kalanchoe daigremontiana and Aloe arborescens on the metabolism of human multiple myeloma cells. *Biointerface Research in Applied Chemistry* **2021**, *11*, 13171–13186, https://doi.org/10.33263/BRIAC115.1317113186.
8. Bozorov, K.; Zhao, J.; Aisa, H.A. 1,2,3-Triazole-containing hybrids as leads in medicinal chemistry: A recent overview, *Bioorganic and Medicinal Chemistry* **2019,** *27*, 3511–3531, https://doi.org/10.1016/j.bmc.2019.07.005.
9. Ashok, D.; Thara, G.; Dharavath, R.; Kirankumar, B.; Sarasija, M.; Bhima, B. Microwave Assisted Synthesis of Flavonoid Based 1,2,3-Triazole and Isoxazole Derivatives, Their Antibacterial, Antioxidant, and Anticancer Activities. *Russian Journal of General Chemistry* **2022**, *92*, 718-724, https://doi.org/10.1134/S1070363222040132.

10. Vani, I.; Prasad, K.R.S. Design, Synthesis, Antimicrobial, and Antioxidant Activity of Dimers of Chromene Containing 1,2,3-Triazole Derivatives Bearing an Alkyl Spacer. *Russian Journal of General Chemistry* **2019**, *89*, 2108-2114, https://doi.org/10.1134/S1070363219100190.
11. Kaushik, C.P.; Pahwa, A.; Singh, D.; Kumar, K.; Luxmi, R. Efficient synthesis, antitubercular and antimicrobial evaluation of 1,4-disubstituted 1,2,3-triazoles with amide functionality. *Monatshefte für Chemie - Chemical Monthly* **2019**, *150*, 1127-1136, http://dx.doi.org/10.1007/s00706-019-2361-9.
12. Khazir, J.; Mir, B.A.; Chashoo, G.; Pilcher, L.; Riley, D. Synthesis and anticancer activity of N-9- and N-7-substituted 1,2,3 triazole analogues of 2,6-di-substituted purine. *Medicinal Chemistry Research* **2020**, *29*, 33-45, https://doi.org/10.1007/s00044-019-02456-9.
13. Klebe, G. Comparative molecular similarity indices analysis: CoMSIA. *Perspectives in Drug Discovery and Design* **1998**, *12*, 87-104, https://doi.org/10.1023/A:1017025803403.
14. Gao, J.; Wang, Y.; Li, K. Comparative analysis of compound NSC13728 as Omomyc homodimer stabilizer by molecular dynamics simulation and MM/GBSA free energy calculation. *Journal of Molecular Modeling* **2022**, *28*, 0948-5023, https://doi.org/10.1007/s00894-022-05082-2.
15. Lokhande, K.B.; Ghosh, P.; Nagar, S.; Venkateswara Swamy, K. Novel B, C-ring truncated deguelin derivatives reveals as potential inhibitors of cyclin D1 and cyclin E using molecular docking and molecular dynamic simulation. *Molecular diversity* **2022**, *26*, 2295-2309, https://doi.org/10.1007/s11030-021-
16. Jiang, D.; Lei, T.; Wang, Z.; Shen, C.; Cao, D.; Hou, T. ADMET evaluation in drug discovery. 20. Prediction of breast cancer resistance protein inhibition through machine learning. *Journal of Cheminformatics* **2020**, *12*, 1758-2946, https://doi.org/10.1186/s13321-020-00421-y.
17. Hadni, H.; Elhallaoui, M. 3D-QSAR, docking and ADMET properties of aurone analogues as antimalarial agents. *Heliyon* **2020**, *6*, 35-80, https://doi.org/10.1016/j.heliyon.2020.e03580.
18. S. TRIPOS Association, Inc 2016. Gaussian Molecular Modeling Software Packages. Version 09. (Accessed March 28, **2022**). https://kasmadtrips.jimdofree.com/.
19. Ge, F.; Qiao, Q.; Chen, X.; Wu, Y. Probing the catalytic activity of M-N4−xOx embedded graphene for the oxygen reduction reaction by density functional theory. *Frontiers of Chemical Science and Engineering* **2021**, *15*, 1206-1216, https://doi.org/10.1007/s11705-020-2017-7.
20. Ueta, I.; Sumiya, K.; Fujimura, K.; Yoshimura, T.; Kikuchi, R.; Saito, Y.; Kawata, K. Extraction of Volatile Anticancer Drugs in Air Using a Solid-Phase Extraction Type Device Followed by Gas Chromatography–Mass Spectrometric Analysis. *Analytical Sciences* **2021**, *37*, 341-345, https://doi.org/10.2116/analsci.20P311.
21. Chanana, G.; Batra, K. Investigating functional performance and substituent effect in modelling molecular structure, UV-visible spectra, and optical properties of D-π-A conjugated organic dye molecules: a DFT and TD-DFT study. *Journal of Molecular Modeling* **2021**, *27*, https://doi.org/10.1007/s00894-021-04824-y.
22. Pagare, P.P.; Morris, A.; Li, J.; Zhang, Y. Development of structure-based pharmacophore to target the β-catenin-TCF protein–protein interaction. *Medicinal Chemistry Research* **2021**, *30*, 429-439, https://doi.org/10.1007/s00044-020-02693-3.
23. Tsai, K.-C.; Chen, Y.-C.; Hsiao, N.-W.; Wang, C.-L.; Lin, C.-L.; Lee, Y.-C.; Li, M.; Wang, B. A comparison of different electrostatic potentials on prediction accuracy in CoMFA and CoMSIA studies. *European Journal of Medicinal Chemistry* **2010**, *45*, 1544-1551, https://doi.org/10.1016/j.ejmech.2009.12.063.
24. Zaim, M.; Kara, I.; Muduroglu, A. Black carrot anthocyanins exhibit neuroprotective effects against MPP+ induced cell death and cytotoxicity via inhibition of oxidative stress mediated apoptosis. *Cytotechnology* **2021**, *73*, 827-840, https://doi.org/10.1007/s10616-021-00500-4.
25. Fiege, S.; Walther, A.; Griewank, A. An algorithm for nonsmooth optimization by successive piecewise linearization. *Mathematical Programming* **2019**, *177*, 343-370, https://doi.org/10.1007/s10107-018-1273-5.
26. Kim, K.H.; Greco, G.; Novellino, E. A critical review of recent CoMFA applications. *Perspectives in Drug Discovery and Design* **1998**, *12*, 257-315, https://doi.org/10.1023/A:1017010811581.
27. Cramer, R.D.; Patterson, D.E.; Bunce, J.D. Comparative molecular field analysis (CoMFA). 1. Effect of shape on binding of steroids to carrier proteins. *Journal of the American Chemical Society* **1988**, *110*, 5959-5967, https://doi.org/10.1021/ja00226a005.
28. Pin, J.-P. Moduler l'action du glutamate dans le cerveau: de nouvelles pistes ouvertes grâce aux récepteurs métabotropiques. *PSN* **2005**, *3*, 132-142, https://doi.org/10.1007/BF03005833.
29. Hocine, S. Design et synthèse des composés azabicycliques contraints De la chimie médicinale à la catalyse, Composites. *Université de Montréal* **2020,** *68*, 1–12.
30. Sharma, R.; Dhingra, N.; Patil, S. CoMFA, CoMSIA, HQSAR and Molecular Docking Analysis of Ionone-based Chalcone Derivatives as Antiprostate Cancer Activity. *Indian journal of pharmaceutical sciences* **2016**, *78*, 54-64, https://doi.org/10.4103/0250-474x.180251.
31. Vishwakarma, K.; Bhatt, H. Molecular modelling of quinoline derivatives as telomerase inhibitors through 3D-QSAR, molecular dynamics simulation, and molecular docking techniques. *Journal of Molecular Modeling* **2021**, *27*, https://doi.org/10.1007/s00894-020-04648-2.
32. Klebe, G.; Abraham, U.; Mietzner, T. Molecular Similarity Indices in a Comparative Analysis (CoMSIA) of Drug Molecules to Correlate and Predict Their Biological Activity. *Journal of Medicinal Chemistry* **1994**, *37*, 4130-4146, https://doi.org/10.1021/jm00050a010.

33. Kordestani, M.D.; Naghibi, S.A.; Hashemi, H.; Ahmadi, K.; Kalantar, B.; Pradhan, B. Groundwater potential mapping using a novel data-mining ensemble model. *Hydrogeology Journal* **2019**, *27*, 211-224, https://doi.org/10.1007/s10040-018-1848-5.
34. Pastor, M.; Cruciani, G.; Clementi, S. Smart Region Definition: A New Way To Improve the Predictive Ability and Interpretability of Three-Dimensional Quantitative Structure−Activity Relationships. *Journal of Medicinal Chemistry* **1997**, *40*, 1455-1464, https://doi.org/10.1021/jm9608016.
35. Ferreira, M.M.C. Multivariate QSAR. *Journal of the Brazilian Chemical Society* **2002,** *13*, 742–753, https://doi.org/10.1590/S0103-50532002000600004.
36. Tropsha, A.; Gramatica, P.; Gombar, V.K. The Importance of Being Earnest: Validation is the Absolute Essential for Successful Application and Interpretation of QSPR Models. *QSAR & Combinatorial Science* **2003**, *22*, 69-77, https://doi.org/10.1002/qsar.200390007.
37. Li, G.; Wang, Y.; Shen, Y.; Guo, H.; He, Q.; Hu, Y.; Liu, H.; Lin, Z.; Wang, Y. In silico design of antimicrobial oligopeptides based on 3D-QSAR modeling and bioassay evaluation. *Medicinal Chemistry Research* **2021**, *30*, 2030-2041, https://doi.org/10.1007/s00044-021-02789-4.
38. Kuz'min, V.; Artemenko, A.; Ognichenko, L.; Hromov, A.; Kosinskaya, A.; Stelmakh, S.; Sessions, Z.L.; Muratov, E.N. Simplex representation of molecular structure as universal QSAR/QSPR tool. *Structural Chemistry* **2021**, *32*, 1365-1392, https://doi.org/10.1007/s11224-021-01793-z.
39. Chtita, S.; Aouidate, A.; Belhassan, A.; Ousaa, A.; Taourati, A.I.; Elidrissi, B.; Ghamali, M.; Bouachrine, M.; Lakhlifi, T. QSAR study of N-substituted oseltamivir derivatives as potent avian influenza virus H5N1 inhibitors using quantum chemical descriptors and statistical methods. *New Journal of Chemistry* **2020**, *44*, 1747-1760, https://doi.org/10.1039/C9NJ04909F.
40. Wunsch, F.M.; Wünsch, B.; Bernal, F.A.; Schmidt, T.J. Quantitative Structure–Activity Relationships of Natural-Product-Inspired, Aminoalkyl-Substituted 1-Benzopyrans as Novel Antiplasmodial Agents. *Molecules* **2021**, *26*, https://doi.org/10.3390/molecules26175249.
41. Golbraikh, A.; Tropsha, A. Beware of q2! *Journal of Molecular Graphics and Modelling* **2002**, *20*, 269-276, https://doi.org/10.1016/S1093-3263(01)00123-1.
42. Pratim Roy, P.; Paul, S.; Mitra, I.; Roy, K. On Two Novel Parameters for Validation of Predictive QSAR Models. *Molecules* **2009**, *14*, 1660-1701, https://doi.org/10.3390/molecules14051660.
43. Roy, K.; Mitra, I.; Kar, S.; Ojha, P.K.; Das, R.N.; Kabir, H. Comparative Studies on Some Metrics for External Validation of QSPR Models. *Journal of Chemical Information and Modeling* **2012**, *52*, 396-408, https://doi.org/10.1021/ci200520g.
44. Halima, H.; Tabti, K; En-Nahli, F.; Bouamrane, S.; Lakhlifi, T; Ajana, M,A.; Bouachrine, M. In Silico Investigation on the Beneficial Effects of Medicinal Plants on Diabtes and Obesitv: Molecular Docking Dynamic Simulations, and ADMET Studies. *Journal of Bionterface Research in Applied Chemistry* **2022**, *11*, 6933-6949, Kadukova, M.; Chupin, V.; Grudinin, S. Docking rigid macrocycles using Convex-PL, AutoDock Vina, and RDKit in the D3R Grand Challenge 4. *Journal of Computer-Aided Molecular Design* **2020**, *34*, 191-200, https://doi.org/10.1007/s10822-019-00263-3.
45. Sun, R.; Zhang, W.; Li, Q.; Li, Y. Inhibition of Bioconcentration of Pentachlorobenzene in the Aquatic Food Chain Based on 3D-QSAR, Molecular Docking, and Molecular Dynamics Simulation. *Water, Air, & Soil Pollution* **2021**, *232*, https://doi.org/10.1007/s11270-021-05000-x.
46. Dassalut Systemes BIOVIA, Discovery Studio Life Science Modeling, Release 2020. San Diego: Dassault Systémes **2020**. https://discover.3ds.com/discovery-studio-visualizer-download.
47. DeLano, W.L. Pymol: An Open-Source Molecular Graphics Tool. *CCP4 Newsl. Protein Crystallogr.* **2002**, *40*, 82–92.
48. Schlander, M.; Hernandez, V.K.; Cheng, C.Y.; Mestre, F.J.; Baumann, M. How Much Does It Cost to Research and Develop a New Drug? A Systematic Review and Assessment. *J. PharmacoEconomics* **2021**, *10*, https://doi.org/10.1007/s40273-021-01065-y.
49. El-Khatabi, K.; El-Mernissi, R.; Aanouz, I. Benzimidazole Derivatives in Identifying Novel Acetylcholinesterase Inhibitors: A Combination of 3D-QSAR, Docking and Molecular Dynamics Simulation. *Phy. Chem. Res.* **2022**, *10*, 237-249.
50. Sangshetti, J.N.; Shaikh, R.I.; Khan, F.A.K.; Patil, R.H.; Marathe, S.D.; Gade, W.N.; Shinde, D.B. Synthesis, antileishmanial activity and docking study of N′-substitutedbenzylidene-2-(6,7-dihydrothieno[3,2-c]pyridin-5(4H)-yl)acetohydrazides. *Bioorganic & Medicinal Chemistry Letters* **2014**, *24*, 1605-1610, https://doi.org/10.1016/j.bmcl.2014.01.035.
51. Younas, A.; Gu, H.; Zhao, Y.; Zhang, N. Novel approaches of the nanotechnology-based drug delivery systems for knee joint injuries: A review. *International Journal of Pharmaceutics* **2021**, *608*, https://doi.org/10.1016/j.ijpharm.2021.121051.
52. Ferreira, L.L.G.; Andricopulo, A.D. ADMET modeling approaches in drug discovery. *Drug Discovery Today* **2019**, *24*, 1157-1165, http://dx.doi.org/10.1016/j.drudis.2019.03.015.
53. He, L.; Jurs, P.C. Assessing the reliability of a QSAR model's predictions. *Journal of Molecular Graphics and Modelling* **2005**, *23*, 503-523, https://doi.org/10.1016/j.jmgm.2005.03.003.
54. El Aissouq, A.; Bouachrine, M.; Ouammou, A.; Khalil, F. Homology modeling, virtual screening, molecular docking, molecular dynamic (MD) simulation, and ADMET approaches for identification of natural anti-

Parkinson agents targeting MAO-B protein. *Neuroscience Letters* **2022**, *786*, 0304-3940. https://doi.org/10.1016/j.neulet.2022.136803.
55. Belhassan, A.; Chtita, S.; Zaki, H.; Alaqarbeh, M.; Alsakhen, N.; Almohtaseb, F.; Lakhlifi, T.; Bouachrine, M. In silico detection of potential inhibitors from vitamins and their derivatives compounds against SARS-CoV-2 main protease by using molecular docking, molecular dynamic simulation and ADMET profiling. *Journal of Molecular Structure* **2022**, *1258*, 0022-2860, https://doi.org/10.1016/j.molstruc.2022.132652.
56. Krstajic, D.; Buturovic, L.J.; Leahy, D.E.; Thomas, S. Cross-validation pitfalls when selecting and assessing regression and classification models. *Journal of Cheminformatics* **2014**, *6*, 1316-1322, https://doi.org/10.1186/1758-2946-6-10.
57. Yap, W.H.; Ahmed, N.; Lim, Y.M. Inhibition of Human Group IIA-Secreted Phospholipase A2 and THP-1 Monocyte Recruitment by Maslinic Acid. *Lipids* **2016**, *51*, 1153-1159, https://doi.org/10.1007/s11745-016-4186-1.
58. Mishra, S.; Rashmi, D. In vitro ADME studies of TUG-891, a GPR-120 inhibitor using SWISS ADME predictor. *Journal of Drug Delivery and Therapeutics* **2019**, *9*, 366-369.
59. Pires, D.E.V.; Blundell, T.L.; Ascher, D.B. pkCSM: Predicting Small-Molecule Pharmacokinetic and Toxicity Properties Using Graph-Based Signatures. *Journal of Medicinal Chemistry* **2015**, *58*, 4066-4072, https://doi.org/10.1021/acs.jmedchem.5b00104.
60. Cao, D.; Wang, J.; Zhou, R.; Li, Y.; Yu, H.; Hou, T. ADMET Evaluation in Drug Discovery. 11. PharmacoKinetics Knowledge Base (PKKB): A Comprehensive Database of Pharmacokinetic and Toxic Properties for Drugs. *Journal of Chemical Information and Modeling* **2012**, *52*, 1132-1137, https://doi.org/10.1021/ci300112j.
61. Wyss, D.F. Structure-guided applications in drug discovery. *British Journal of Cancer* **2003,** *8*, 924–926.
62. Clark, D.E. In silico prediction of blood–brain barrier permeation. *Drug Discovery Today* **2003,** *8*, 927–933, https://doi.org/10.1016/S1359-6446(03)02827-7.
63. Patel, K.; M.J. Kirkpatrick, C. Pharmacokinetic Concepts Revisited - Basic and Applied. *Current Pharmaceutical Biotechnology* **2011**, *12*, 1983-1990, https://doi.org/10.2174/138920111798808400.
64. Pryor, W.A. Cytochrome P450: Structure, mechanism, and biochemistry. *Free Radical Biology Medicine* **1996,** *21*.
65. Šrejber, M.; Navrátilová, V.; Paloncýová, M.; Bazgier, V.; Berka, K.; Anzenbacher, P.; Otyepka, M. Membrane-attached mammalian cytochromes P450: An overview of the membrane's effects on structure, drug binding, and interactions with redox partners. *Journal of Inorganic Biochemistry* **2018**, *183*, 117-136, https://doi.org/10.1016/j.jinorgbio.2018.03.002.
66. Nixon, G.L.; Moss, D.M.; Shone, A.E.; Lalloo, D.G.; Fisher, N.; O'Neill, P.M.; Ward, S.A.; Biagini, G.A. Antimalarial pharmacology and therapeutics of atovaquone. *Journal of Antimicrobial Chemotherapy* **2013**, *68*, 977-985, https://doi.org/10.1093/jac/dks504.